

Microstructure and Wear Resistance of FeCrBSi Plasma-Sprayed Coating Remelted by Gas Tungsten Arc Welding Process

Dong Tianshun, Zheng Xiaodong, Li Yalong, Li Guolu, Zhou Xiukai, and Wang Haidou

(Submitted November 16, 2017; in revised form April 22, 2018; published online July 6, 2018)

Herein, an FeCrBSi coating was fabricated via plasma spray on AISI1045 steel, and subsequently, a gas tungsten arc welding (GTA) process was employed to remelt the coating. The microstructure, microhardness, fracture toughness and surface roughness of the coating before and after remelting were investigated, as well as the wear resistance was tested by a UMT-3-type sliding wear apparatus. The results showed that, upon remelting, most defects in the as-sprayed coating were effectively eliminated, the surface roughness decreased by 43%, and the coating–substrate interface bonding changed from mechanical to metallurgical. The phase composition of the as-sprayed coating was primarily α -Fe and a small amount of hard Fe_3B phase, while the remelted coating consisted of α -Fe and $(\text{Fe,Cr})_{23}\text{C}_6$ and a small quantity of CrB. In addition, remelting the coating was found to induce a 287.6% increase in the fracture toughness, a 33.4% increase in the average microhardness, and a 47.5% decrease in the wear volume, while the failure mechanism changed from abrasive wear to fatigue wear upon remelting. Therefore, GTA remelting of plasma-sprayed coating was found to be a feasible method to obtain a coating with good wear resistance.

Keywords FeCrBSi, GTA remelting, microstructure, plasma spray, wear resistance

1. Introduction

As the most common self-fluxing alloy coating, the FeCrBSi coating is widely used in metallurgy, mining, power, engineering machinery and other fields owing to its high hardness and good wear resistance (Ref 1, 2). However, like many other thermal spray coatings, the microstructure of the FeCrBSi coating exhibits pores, microcracks, unmelted particles and a lamellar structure (Ref 3, 4). Moreover, the adhesion strength between the coating and substrate is relatively low because of the mechanical bonding at the interface (Ref 5-7). Thus, the wear resistance and fatigue resistance of the coating are decreased (Ref 8-10). In recent years, many researchers have studied treating the thermal spray coating with remelting and have found it an effective treatment method to improve the quality and to enhance the performance of the ceramic coating (Ref 11, 12), cermet coating (Ref 13, 14) and metal coating (Ref 15, 16). There are many studies on the remelting of NiCrBSi metal coating (Ref 17, 18); nonetheless, few reports

on the effects of the remelting treatment of the FeCrBSi metal coating have been published so far.

Among the current remelting processes (Ref 19-23), the gas tungsten arc welding (GTA) process has many obvious advantages such as low cost of equipment, good protection of an inert gas, a low heat input, shallow penetration and easy to be popularized and applied (Ref 24). In this paper, therefore, the plasma-sprayed FeCrBSi coating was remelted by the GTA process and the microstructure and wear resistance were studied. This research has reference value for preparing a coating with good wear resistance.

2. Experimental Procedure

2.1 Raw Material

The AISI 1045 steel was quenched and tempered before its use herein as a substrate with the dimensions of 60 mm \times 30 mm \times 10 mm. An Fe-based self-fluxing alloy powder (purity > 99.5%) was used for plasma spray whose particle size ranged from 10 to 25 μm . The chemical compositions of the Fe-based self-fluxing alloy powder and the substrate are shown in Table 1, while the morphology of the spray powder is shown in Fig. 1.

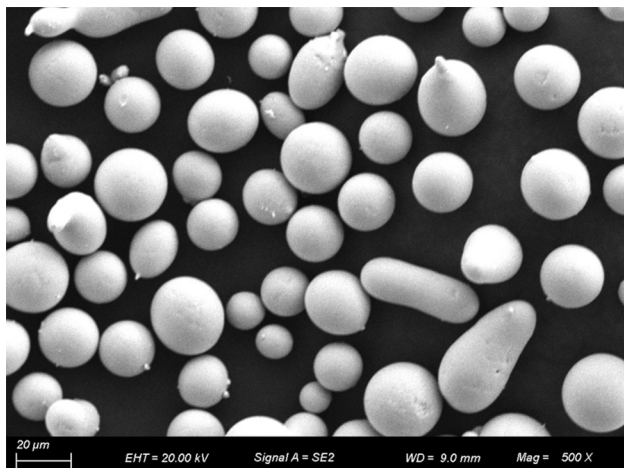
2.2 Experimental Method

Prior to spraying, the substrate was grit-blasted with silica sand and cleaned ultrasonically for 30 min in a bath of acetone to obtain the required roughness and to remove any surface oxides or grease. The spraying powder was heated to 353 K with a keeping time of 4 h, whereupon the FeCrBSi coating was fabricated via plasma-sprayed equipment (GP-80, Jiujiang, China). Subsequently, the as-sprayed coating was remelted using a tungsten arc welding machine (YC-300WX, Pana-

Dong Tianshun, Li Guolu, and Zhou Xiukai, School of Material Science and Engineering, Hebei University of Technology, Tianjin 300130, China; Zheng Xiaodong and Li Yalong, School of Material Science and Engineering, Hebei University of Technology, Tianjin 300130, China; and National Key Laboratory for Remanufacturing, Academy of Armored Forces Engineering, Beijing 100072, China; and Wang Haidou, National Key Laboratory for Remanufacturing, Academy of Armored Forces Engineering, Beijing 100072 China. Contact e-mails: liguolu0305@163.com and wanghaidou@aliyun.com.

Table 1 Compositions of Fe-based self-fluxing alloy powder and substrate

Weight, %	C	Cr	Ni	B	Si	Mn	RE	Fe
Fe-based alloy	...	12	0.3	2.5	1	0.3	1	Bal.
AISI 1045 steel	0.45	0.25	0.66	...	Bal.

**Fig. 1** The morphology of spray powder

sonic). The parameters used for the grit blasting, spraying and remelting processes are shown in Table 2. Finally, the sliding wear resistance and coefficient of friction were tested by a ball-on-disk-type sliding wear apparatus (UMT-3, Bruker Corp.). To ensure uniform experimental conditions, both the as-sprayed and remelted samples were polished prior to the wear test with grinding papers progressing from 200# to 1000# grade to achieve a surface roughness of less than 0.8 μm . The ball of the sliding wear apparatus was made of GCr15 steel with a diameter of 6 mm and was operated with a maximum load of 30 N, a holding time of 30 min, a frequency of 10 Hz and a stroke length of 4 mm.

2.3 Detection and Analysis

Microstructural observations and chemical elemental analysis of the coating cross sections before and after remelting were carried out by a field-emission scanning electron microscope (SEM; Hitachi S4800) equipped with an energy-dispersive x-ray spectrometer (EDS; NORAN Vantage, Noran Instruments Inc.). Using the SEM images, the average porosity of ten micrographs (1000 times magnification) was measured using the Image J2x image analysis software. The phase composition of the coatings was evaluated by x-ray diffraction (XRD: D/Max 2500PC, Rigaku Corp.). The microhardness and fracture toughness were measured by a microhardness tester (HMV-2000, Shimadzu) with an applied load of 0.98 and 9.8 N for 15 s dwell time, respectively, where the reported microhardness values were averaged from at least three measurements. The three-dimensional morphology of the wear scars and surface roughness of the coatings were observed by a surface profiler (Phase Shift MicroXAM-3D, KLA-Tencor).

Table 2 The process parameters of grit blasting, spraying and remelting

Process	Parameters	Values
Grit blasting	Air pressure, MPa	0.7
	Blasting distance, mm	300
	Blasting angle, $^{\circ}$	45
Plasma spraying	Voltage, V	60
	Current, A	500
	Spraying distance, mm	150
	Cooling of substrate	Air blow
	Gas flow rate, L/min	Ar 80 H ₂ 10
GTA remelting	Coating thickness, mm	0.35-0.4
	Current, A	70
	Arc length, mm	2
	Argon flow, L/min	10
	Scanning speed, mm/min	200
	Step size, mm	2

3. Results and Discussion

3.1 Micromorphology of Coatings

The SEM images of the morphological characteristics of the as-sprayed and remelted coating cross sections are shown in Fig. 2. It is evident that the internal structure of the as-sprayed coating was layered, where the layers were about 55.8 μm long and 6.2 μm wide. As well as, a large number of defects were observed, such as pores, microcracks, inclusions and unmelted particles about 3.6-6.7 μm in diameter. The average porosity of the as-sprayed coatings, as measured by Image J2x, was 4%. Additionally, a gap exists between the as-sprayed coating and the substrate (Fig. 2a) about 41.9 μm in width, and the type of bonding at the coating-substrate interface was a mechanical combination.

In contrast, the internal structure of the remelted coating was more compact than the as-sprayed coating owing to the reduction of pores, cracks and inclusions, where the average porosity of the remelted coating was 0.4%. Therefore, the density of the as-sprayed coating was significantly improved by the remelting treatment. Moreover, a diffusion transfer belt (DTB) about 13.7 μm thick was formed between the remelted coating and the substrate (Fig. 2b), and the type of bonding at the interface was a metallurgical combination (Ref 25, 26).

To study the trend of the chemical element variation at the interface, EDS line-scan mapping was carried out across the interface of the as-sprayed and remelted coatings, as shown in Fig. 3. On the as-sprayed coating sample, the Cr, Si and Fe elements were observed to abruptly change from the substrate to the coating layer owing to the mechanical bonding of the as-sprayed coating and the substrate. On the remelted coating sample, however, the Cr, Si and Fe elements were observed to exhibit a gradual change from the substrate to the coating layer,

indicating the occurrence of dissolution and diffusion and the formation of a strong metallurgical bonding.

It is noted that the concentration gradient of Cr, Si and B in the area between the as-sprayed coating and the substrate is higher than that at other locations. During the remelting process, Cr, Si and B can easily diffuse from the high-temperature molten layer into the semi-molten substrate. Because the atomic radius of Cr is larger than that of Si and B, Cr is selected as an example to explain the elemental migration phenomenon during the remelting process. According to the second Fick's diffusion law, $(C - C_0)/(C_s - C_0) = \text{erf}[X/2(Dt)^{1/2}]$, where C_s (12%) and C_0 (0%) are the concentrations of Cr in the remelted coating and the substrate, respectively; C is the concentration of Cr in the substrate after diffusion; X is the diffusion distance (10 μm); D is diffusion coefficient of Cr ($3.476 \times 10^{-14} \text{ m}^2 \text{ s}^{-1}$); and t is the diffusion time (1200 s). After calculation, the concentration of Cr at 10 μm distance from the interface is 0.41%, which is in accordance with the EDS results at Position A in Fig. 3(b): 92.13 Fe, 0.44 Cr, 5.27 C, 0.31 Si, 1.85 B (wt%).

Figure 4 displays the high-mag images of the remelted coating at the interface, and it can be found that the interface between the diffusion layer and the substrate is obviously uneven. The morphology of the diffusion layer is indented and has a tendency to spread continuously. Due to the short solidification time, the growth of new phase caused by diffusion is limited. The elemental diffusion not only makes the coating and the substrate realize metallurgical bonding, but also increases the bonded area of the coating and the substrate, so that the remelted coating has a better interface behavior than that of as-sprayed coating.

3.2 Phase Composition of Coatings

The XRD patterns obtained from the as-sprayed and remelted coating samples are shown in Fig. 5. The as-sprayed coating phases are observed to mainly comprise $\alpha\text{-Fe}$ with a small amount of the hard Fe_3B phase. The phase composition of the as-sprayed coating is simple because during the spraying process the metallurgical reaction of the alloy powder is minimal owing to its partial melting. After remelting of the

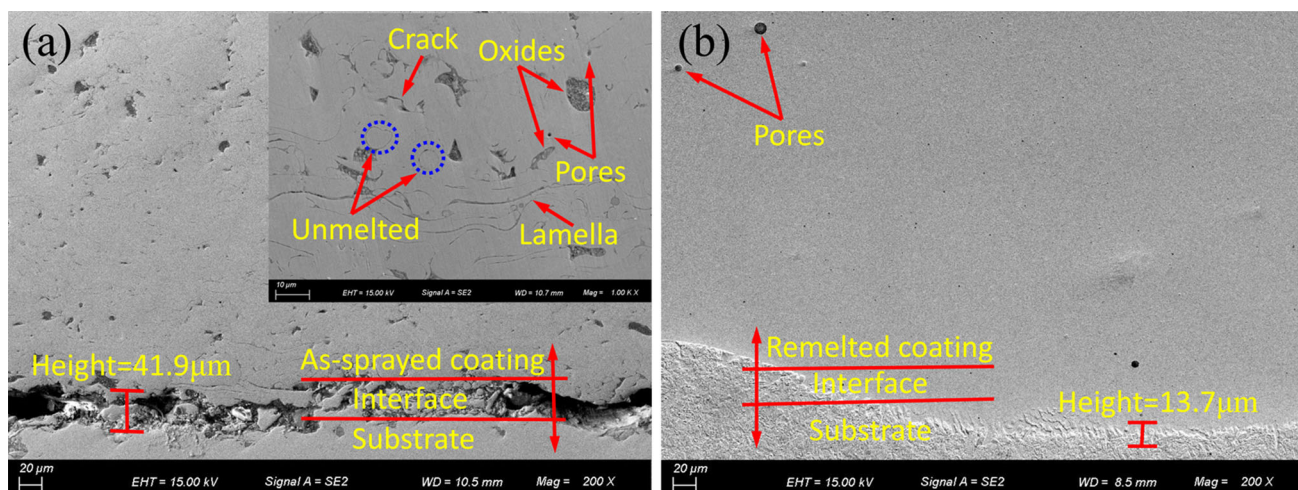


Fig. 2 Cross-sectional SEM morphology of (a) as-sprayed coating and (b) remelted coating

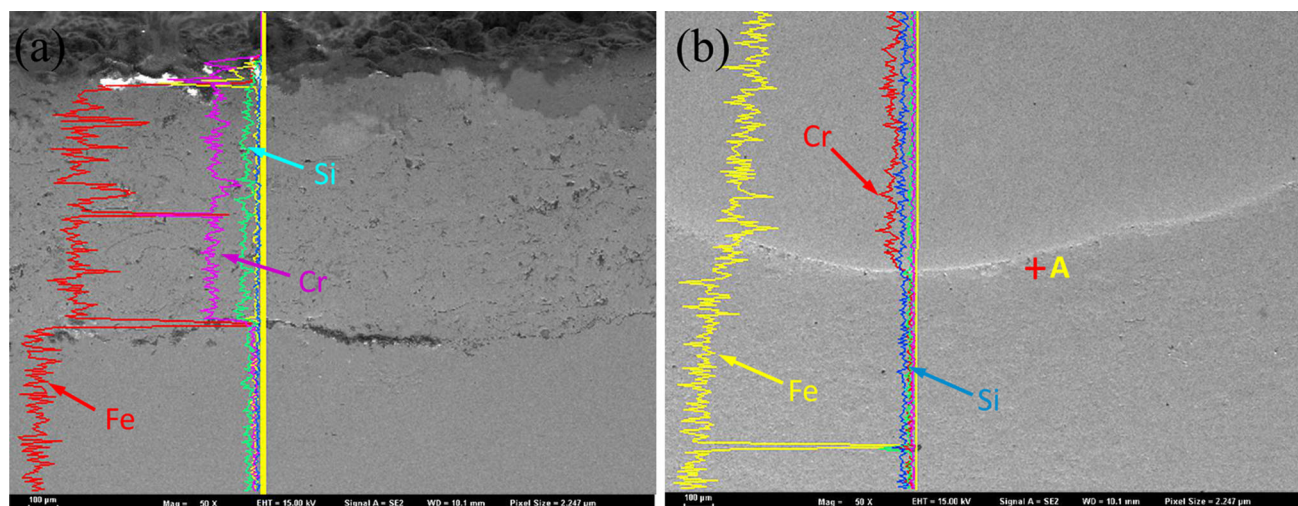


Fig. 3 The EDS line scanning results of (a) as-sprayed coating and (b) remelted coating

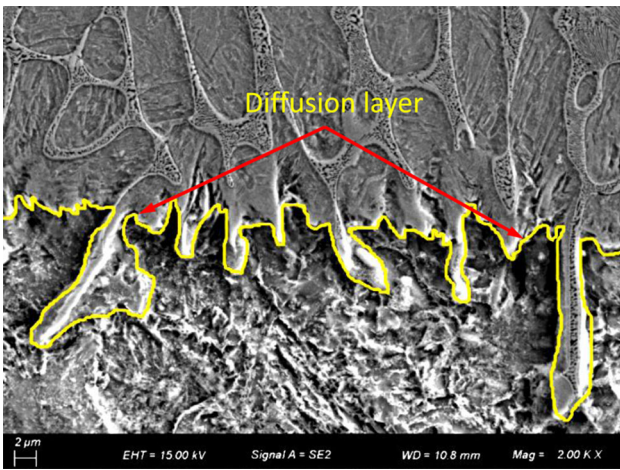


Fig. 4 The high-mag images of the remelted coating at the interface

coating, however, more $(\text{Fe,Cr})_{23}\text{C}_6$ carbide phase and a small amount of CrB were observed. During the remelting process, the coating is completely melted and recrystallized and the conditions are sufficient for a metallurgical reaction, and thus the phase composition of the remelted coating is more complex.

3.3 Microstructure of the Remelted Coating

The microstructure of the remelted coating is shown by SEM images in Fig. 6, where three primary zones can be identified from top to bottom (Fig. 6a), labeled as the remelted coating, the interface layer and the heat-affected zone. The as-sprayed coating is heated to a single-liquid phase completely when the temperature exceeds its liquidus line, whereupon the remelted coating forms after solidification. The local substrate material adjacent to the coating is thus heated to a temperature that is between its solidus line and liquidus line. Therefore, the substrate is partially melted and two-phase regions are formed wherein solid and liquid phases coexist, which becomes the interface layer after solidification. Because the interface layer is composed of a partially molten substrate and the remelted coating, its microstructure, mechanical properties and chemical composition are highly uneven (Ref 27). Although the substrate does not melt completely when the temperature is below its solidus line, the performance and microstructure of the local substrate adjacent to the interface layer are changed and this area was therefore named the heat-affected zone.

The grain boundary structure of the remelted coating is lamellar, as shown in Fig. 6(b), and the EDS of two areas (Points A and B in Fig. 6b) is given in Fig. 6(c) and (d). The results show that the elements at Point A are mainly C and Fe and a small amount of dissolved Cr and Si, while at Point B there exists more Cr in addition to C and Fe. Combining these results with those of XRD (Fig. 5), it can be seen that ellipsoidal-shaped grains are $\alpha\text{-Fe}$ and the grain boundary is comprised of $\alpha\text{-Fe} + (\text{Fe,Cr})_{23}\text{C}_6$ eutectic.

3.4 Microhardness and Fracture Toughness

The average microhardness value of the substrate, as-sprayed coating and remelted coating is 259 $\text{HV}_{0.1}$, 640 $\text{HV}_{0.1}$ and 854 $\text{HV}_{0.1}$, respectively. Thus, the remelting of the as-sprayed coating increased the microhardness of the coating by

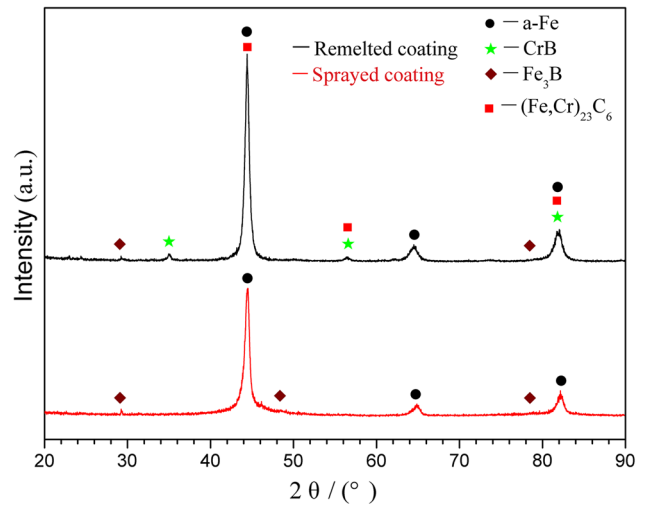


Fig. 5 X-ray diffraction patterns of coatings before and after remelting

33.4%, which is beneficial for the improvement of its wear resistance. This is because, during the remelting and solidification process, many dispersed and fine CrB and $(\text{Fe,Cr})_{23}\text{C}_6$ hard phases are formed in the coating. In addition, during the remelting process, any trapped gas can escape from the melt under the stirring of the arc force, and the deoxidation of the Si and Mn elements reduces the number of oxidation inclusions. This ultimately leads to the microstructure of the remelted coating becoming compact and uniform. Therefore, the hardness of the as-sprayed coating was improved significantly by the remelting process.

The fracture toughness of the coatings was calculated by the Niihara method, and its average values of coatings before and after remelting are found to be 0.355 and 1.376 $\text{MPa m}^{1/2}$, respectively, indicating that the fracture toughness of the coating after remelting is increased by 287.6%. Because fracture toughness is a mechanical property parameter to resist crack propagation, the surface of remelted coating is not easy to lose material and form debris during the wear process. Thus, an increased fracture toughness improves the wear resistance of the remelted coating. In summary, the microhardness and fracture toughness of the coating were distinctly improved after the remelting treatment.

3.5 Surface Roughness

The three-dimensional morphology of the coating obtained by the surface profiler before and after remelting is shown in Fig. 7. The surface of the as-sprayed coating is visibly uneven, while that of the remelted coating is relatively smooth and exhibits a “fish scale” rippling. The surface roughness (R_a) of the as-sprayed coating was measured to be 9.5 μm , while that of the remelted coating was 5.4 μm , exhibiting a 43% decrease. Therefore, the surface quality of the coating was improved significantly by the GTA remelting treatment.

3.6 Wear Resistance

The wear resistance of the coating before and after remelting was studied using friction and wear experiments. Figure 8 presents the friction coefficient curves of the as-sprayed and remelted coatings, where a running stage is observed up to

600 s, at which point the coating enters the stable wear stage. In the running stage, the contact area between the grinding ball and the asperity of the sample surface gradually increased as the wear process continued, and thus the friction coefficient rose sharply. However, as the wear process continued the asperity was sheared to produce debris, which filled the pits and smoothed the contact surface. Thus, the friction coefficient eventually decreased and the wear gradually stabilized. It can be seen from Fig. 8 that the friction coefficient of the remelted coating is 0.45, which is smaller than that of as-sprayed coating (0.53). It is because the microhardness of the remelted coating is greater than that of the as-sprayed coating and so, during the wear process, the asperity of the remelted coating is not fully in contact with the grinding ball.

Figure 9 shows the three-dimensional morphology of the wear scars of the coating before (Fig. 9a) and after (Fig. 9b) remelting, where it appears that the length and width of the wear scar of the as-sprayed coating are greater than that of the remelted coating. The wear scar length values of the as-sprayed and remelted coatings are 5.72 and 4.63 mm, respectively, the width values are 1.25 and 0.88 mm, respectively, and the wear scar depth values are 39.3 and 21.6 μm , respectively. In addition, it can be seen from Fig. 9(c) that the bottom of the wear scar is uneven, revealing that microcracks have propagated into the coating with the continuous cutting of the shear stress during the wear process. This continuous propagation of microcracks will ultimately result in the failure of the coating. A longitudinal section of the wear scar on the remelted coating is shown in Fig. 9(d), where it is seen that the bottom of the

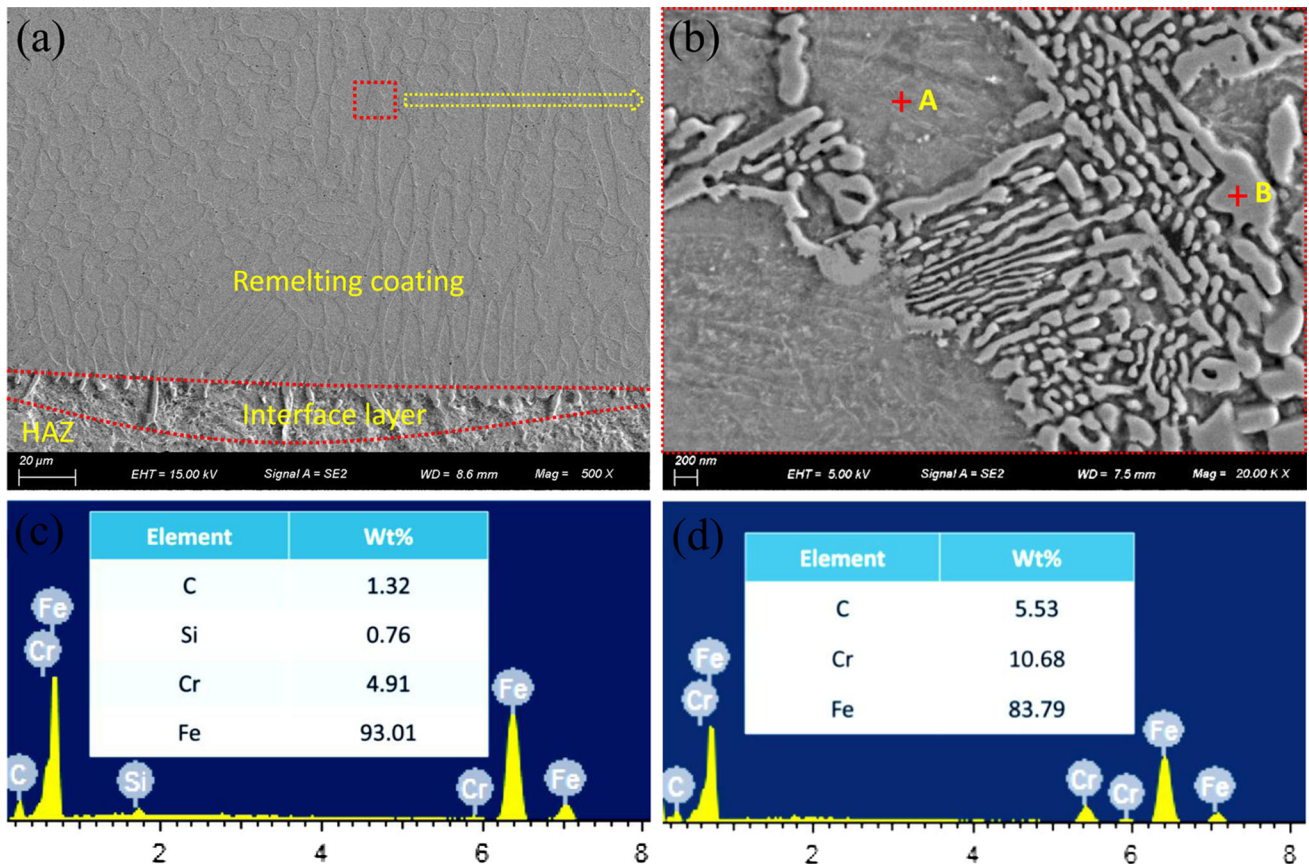


Fig. 6 Microstructure of the remelted coating (a) low magnification microstructure (b) high magnification microstructure (c) the EDS of point A (d) the EDS of point B

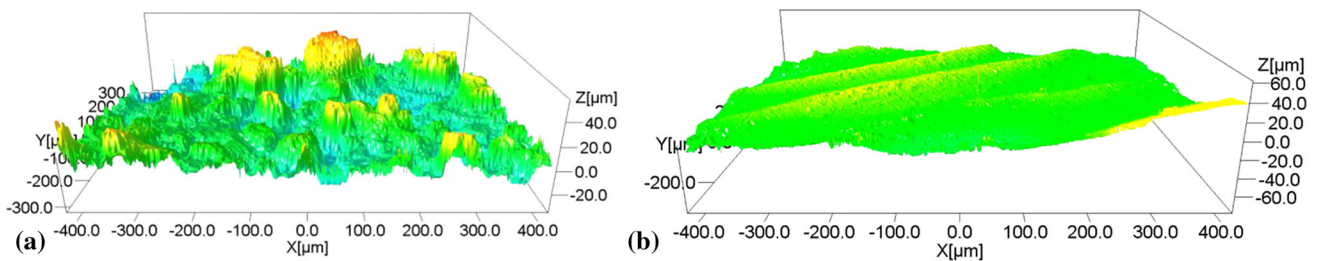


Fig. 7 The surface morphology of (a) as-sprayed coating (b) remelted coating

scar is smooth, indicating that there are few microcracks initiating and propagating during the wear process.

The wear resistance of coating can be calculated by $W = L/V$ (Ref 28), where V is the wear volume, L is the sliding distance, and W is the wear resistance; signifying that the wear resistance has an inverse relationship with the wear volume. Using the three-dimensional morphology profilometer measurements, the wear volume of the as-sprayed and remelted coatings was found to be 4.63×10^7 and $2.43 \times 10^7 \mu\text{m}^3$, respectively, signifying that the remelting treatment decreased the wear volume by 47.5%. Therefore, the wear resistance of the remelted coating is superior to that of the as-sprayed coating.

Figure 10 shows the SEM morphology of the wear scar and the corresponding debris on the as-sprayed (Fig. 10a and b) and remelted (Fig. 10c and d) coating samples. Serious spalling and obvious grooves are evident on the as-sprayed coating (Fig. 10a), but no obvious plastic deformation can be found,

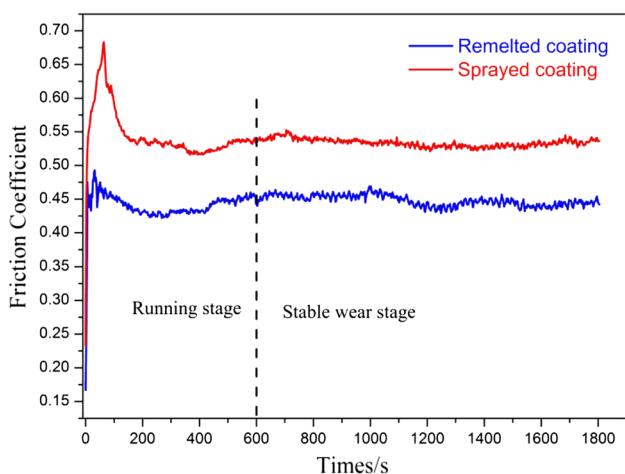


Fig. 8 The friction coefficient curves of coatings before and after remelted coating

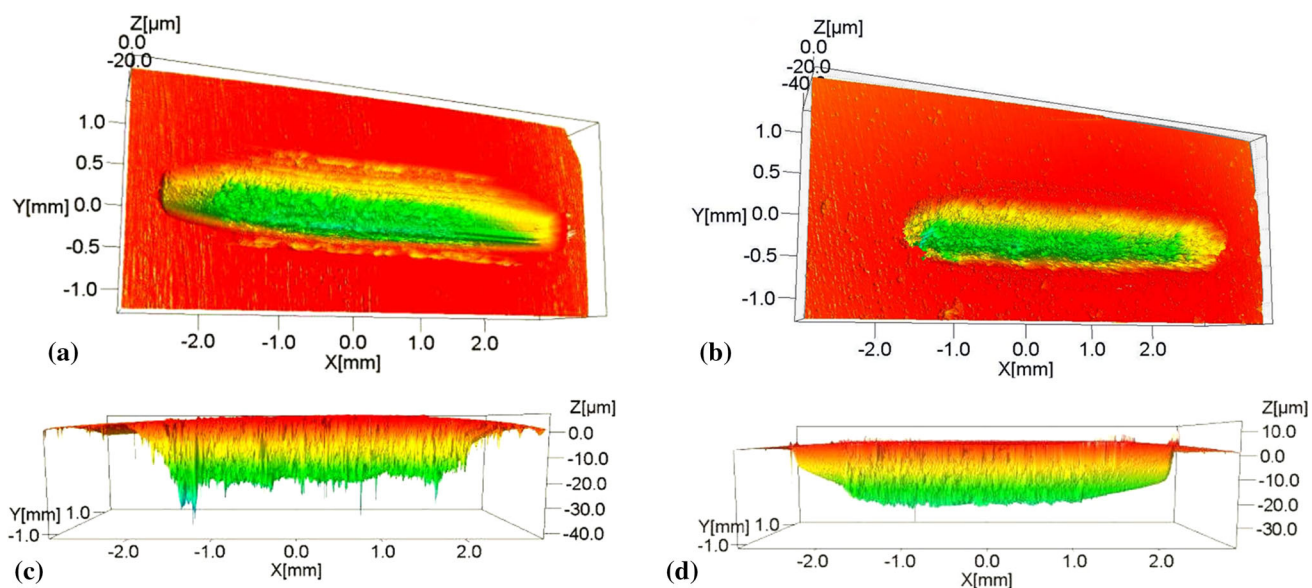


Fig. 9 The three-dimensional morphology of the wear scar (a) as-sprayed coating (b) remelted coating (c) longitudinal section of as-sprayed coating (d) longitudinal section of remelted coating

indicating that the coating exhibits brittle fracture characteristics. Figure 10(b) shows the high-resolution image of the region at Position A in Fig. 10(a), where it is evident that microcracks, spalling pits and lamellar fractures are generated in the wear scar. Because of the inherent layered structure and the presence of pores in the coating, the coating readily develops stress concentration, crack initiation, rapid expansion and, ultimately, delamination under the continuous action of the normal and tangential stress. Further, the spalling debris is crushed into the flaking pits under the action of sliding (Position B in Fig. 10a). The massive debris with different sizes is shown in Fig. 10(e). It is evident that the failure mechanism of the as-sprayed coating is abrasive wear.

Figure 10(c) shows the wear scar morphology for the remelted coating that, compared with the as-sprayed coating, exhibits a lesser degree of wear and no obvious brittle fracture and spalling characteristics. Figure 10(d) shows the high-resolution image of the region at Position C in Fig. 10(c), where pitting and the accumulation of plastic deformation are observed on the wear scar, indicating plastic deformation of the remelted coating during the wear process. Because the frictional surface was not perfectly smooth when the grinding ball came into contact with the remelted coating surface, the coating underwent plastic deformation via the extrusion induced between the grinding ball and sample. As the sliding continued, the temperature of the remelted coating increased and the deformed metal exhibited a plastic rheological phenomena. In addition, the plastic deformation damage gradually accumulated under the repeated action of the grinding ball, whereupon fatigue cracks were initiated until the shear stress exceeded the shear strength of the remelted coating. Further, the fatigue cracks extended to ultimately reach the surface, which created the pitting and the granular uniform debris formed (Fig. 10f). The failure mechanism of the remelted coating is fatigue wear.

Unlike the as-sprayed coating, the remelted coating exhibits a large number of continuous fine reticular hard phases that play a supporting role in the process of wear, where the

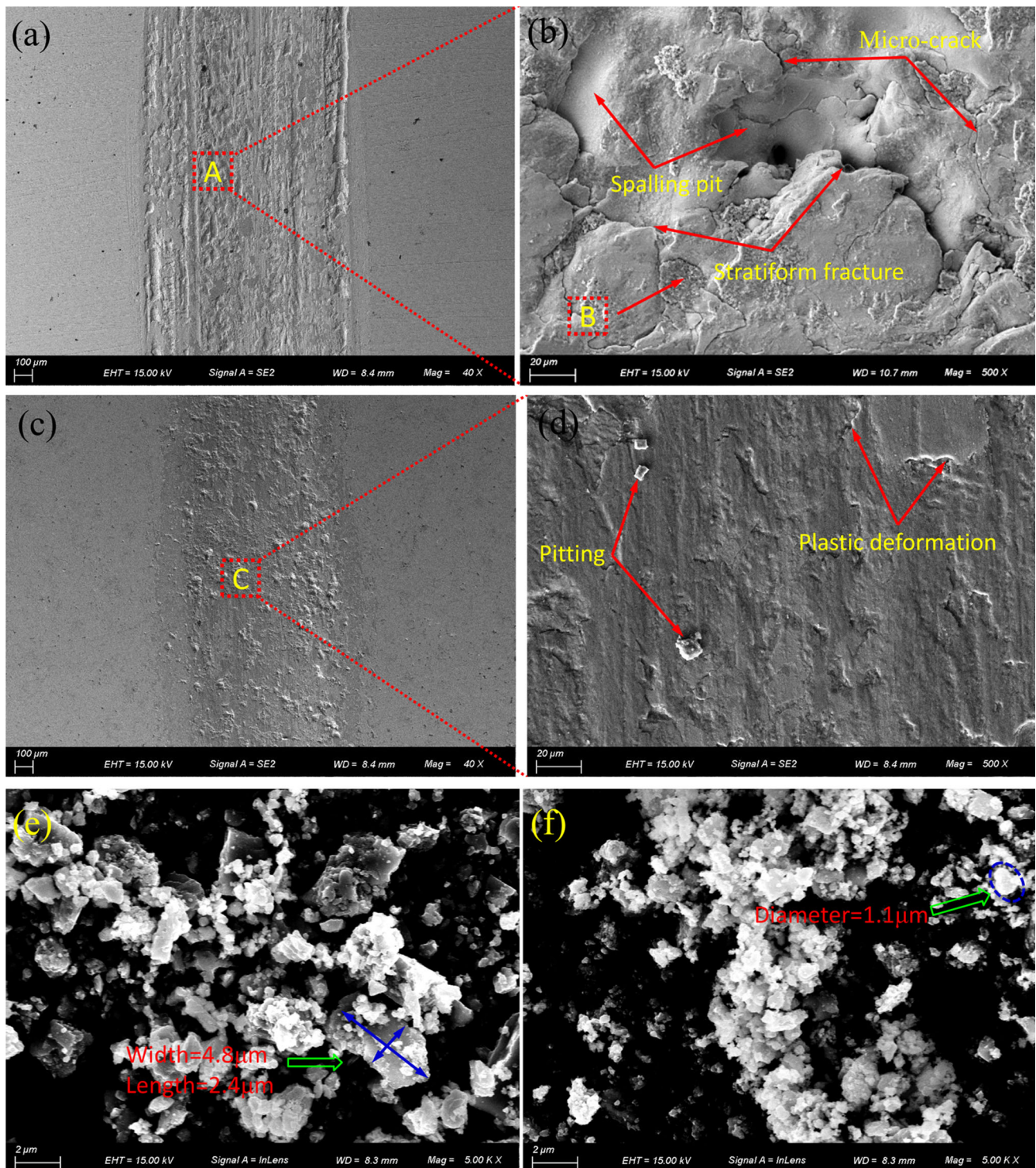


Fig. 10 The SEM morphology of the wear scar and debris (a) wear scar morphology of as-sprayed coating (b) high-resolution image at Position A (c) wear scar morphology of remelted coating (d) high-resolution image at Position C (e) the debris morphology of as-sprayed coating (f) the debris morphology of remelted coating

reticular phase protects the softer α -Fe and, in turn, the α -Fe inhibits the removal of the reticular phase. Moreover, after remelting, the pores and layered structure in the coating are eliminated and the microstructure is compact; thus, the stress concentration is reduced in the wear process. In addition, the increase in fracture toughness is beneficial for the wear resistance of remelted coating in a certain range (Ref 29). It

is because the fracture toughness of the remelted coating is higher than that of as-sprayed coating, the plastic deformation is serious under the action of large local stress. Thus, the normal press at a unit area on the remelted coating is smaller than that on the as-sprayed coating and the depth of the wear scar is relatively shallow. And the propagation velocity of the microcrack decreased with the increase in the fracture tough-

ness. Therefore, the remelted coating has a good wear resistance.

4. Conclusions

In the present work, FeCrBSi plasma-sprayed coating was first prepared on a steel substrate and then remelted by the GTA process. The microstructure, mechanical properties and wear resistance of FeCrBSi coating were studied with the following conclusions:

1. The remelted coating consisted of α -Fe and $(\text{Fe,Cr})_{23}\text{C}_6$ and a small quantity of CrB and Fe_3B , and its microstructure became more uniform and compact, the porosity decreased from 4 to 0.4% with remelting.
2. The fracture toughness and average microhardness of the coating increased with remelting by 287.6 and 33.4%, respectively.
3. The remelted coating had a good wear resistance, and its wear volume decreased by 47.5% with remelting. Therefore, GTA remelting of plasma-sprayed coating was a good method to prepare a coating with excellent wear resistance.

Acknowledgments

This work was financially supported by the National Natural Science Foundation of China (Nos. 51675158, 51535011) and the Natural Science Foundation of Hebei Province (No. E2016202325). We thank Sara Maccagnano-Zacher, Ph.D., from Liwen Bianji, Edanz Editing China (www.liwenbianji.cn/ac), for editing the English text of a draft of this manuscript.

References

1. S.Y. Chen, G.Z. Ma, H.D. Wang, J.J. Kang, B.S. Xu, H.J. Wang, and M. Liu, Investigation of Competing Failure Mechanism and Life of Plasma Sprayed Fe-Based Alloy Coating Under Rolling-sliding Contact Condition, *Tribol. Int.*, 2016, **101**, p 25–32
2. Y. Peng, C. Zhang, H. Zhou, and L. Liu, On the Bonding Strength in Thermally Sprayed Fe-Based Amorphous Coatings, *Surf. Coat. Technol.*, 2013, **218**(1), p 17–22
3. B. Li, Y.M. Gao, M.M. Han, H.J. Guo, J.H. Jia, W.Z. Wang, and H.T. Deng, Tribological Properties of NiAl Matrix Composite Coatings Synthesized by Plasma Spraying Method, *J. Mater. Res.*, 2017, **32**, p 1–8
4. H.S. Nithin, V. Desai, and M.R. Ramesh, Elevated Temperature Solid Particle Erosion Performance of Plasma-Sprayed Co-Based Composite Coatings with Additions of Al_2O_3 and CeO_2 , *J. Mater. Eng. Perform.*, 2017, **11**, p 1–11
5. Q.Y. Hou, Influence of Molybdenum on the Microstructure and Properties of a FeCrBSi Alloy Coating Deposited by Plasma Transferred Arc Hardfacing, *Surf. Coat. Technol.*, 2013, **225**, p 11–20
6. Z.Y. Piao, B.S. Xu, H.D. Wang, and D.H. Wen, Investigation of RCF Failure Prewarning of Fe-Based Coating by Online Monitoring, *Tribol. Int.*, 2014, **72**, p 156–160
7. Z.Q. Zhang, H.D. Wang, B.S. Xu, and G.S. Zhang, Characterization of Microstructure and Rolling Contact Fatigue Performance of NiCrBSi/WC-Ni Composite Coatings Prepared by Plasma Spraying, *Surf. Coat. Technol.*, 2015, **261**, p 60–68
8. Z.Y. Piao, B.S. Xu, H.D. Wang, and C.H. Pu, Influence of Undercoating on Rolling Contact Fatigue Performance of Fe-Based Coating, *Tribol. Int.*, 2010, **43**, p 252–258
9. F. Ghadami, M. Heydarzadeh Sohi, and S. Ghadami, Effect of TIG Surface Melting on Structure and Wear Properties of Air Plasma Sprayed WC-Co Coatings, *Surf. Coat. Technol.*, 2014, **261**, p 108–113
10. Y. Wang, C.G. Li, L.X. Guo, and W. Tian, Laser Remelting of Plasma Sprayed Nanostructured Al_2O_3 - TiO_2 Coatings at Different Laser Power, *Surf. Coat. Technol.*, 2017, **228**, p 1–10
11. J.B. Yu, Y. Wang, F.F. Zhou, L. Wang, and Z.Y. Pan, Laser Remelting of Plasma-Sprayed Nanostructured Al_2O_3 -20wt.% ZrO_2 Coatings onto 316L Stainless Steel, *Appl. Surf. Sci.*, 2018, **431**, p 112–121
12. Y. Wang, C.G. Li, W. Tian, and Y. Yang, Laser Surface Remelting of Plasma Sprayed Nanostructured Al_2O_3 -13wt.% TiO_2 Coatings on Titanium Alloy, *Appl. Surf. Sci.*, 2009, **255**, p 8603–8610
13. G. Marginean and D. Utu, Microstructure Refinement and Alloying of WC-CoCr Coatings by Electron Beam Treatment, *Surf. Coat. Technol.*, 2010, **205**, p 1985–1989
14. K.M. Deen, M. Afzal, Y. Liu, A. Farooq, A. Ahmad, and E. Asselin, Improved Corrosion Resistance of Air Plasma Sprayed WC-12%Co Cermet Coating by Laser Re-melting Process, *Mater. Lett.*, 2017, **191**, p 34–37
15. N. Kang, C. Verdy, P. Coddet, Y.C. Xie, Y.Q. Fu, H.L. Liao, and C. Coddet, Effects of Laser Remelting Process on the Microstructure, Roughness and Microhardness of In Situ Cold Sprayed Hypoeutectic Al-Si Coating, *Surf. Coat. Technol.*, 2017, **318**, p 355–359
16. H.S. Wang, H.G. Chen, Y.T. Liu, and J.S.C. Jang, Application of Laser Remelting Process on the Zr-Cu Based Alloy Composite, *Intermetallics*, 2018, **95**, p 11–18
17. J.B. Chen, Y.C. Dong, L.N. Wan, Y. Yang, Z.H. Chu, J.X. Zhang, J.N. He, and D.Y. Li, Effect of Induction Remelting on the Microstructure and Properties of In Situ TiN-Reinforced NiCrBSi Composite Coatings, *Surf. Coat. Technol.*, 2018, **340**, p 159–166
18. R. Gonzalez, M. Cadenas, R. Fernandez, J.L. Cortizo, and E. Rodriguez, Wear Behaviour of Flame Sprayed NiCrBSi Coating Remelted by Flame or by Laser, *Wear*, 2007, **262**, p 301–307
19. Š. Houdková, E. Smazalová, M. Vostřák, and J. Schubert, Properties of NiCrBSi Coating, as Sprayed and Remelted by Different Technologies, *Surf. Coat. Technol.*, 2014, **253**, p 14–26
20. N. Serres, F. Hlawka, S. Costil, C. Langlade, and F. Machi, Corrosion Properties of In Situ Laser Remelted NiCrBSi Coatings Comparison with Hard Chromium Coatings, *J. Mater. Process Technol.*, 2011, **211**, p 133–140
21. E. Feldshtein, M. Kardapolava, and O. Dyachenko, On the Effectiveness of Multi-component Laser Modifying of Fe-Based Self-Fluxing Coating with Hard Particulates, *Surf. Coat. Technol.*, 2016, **307**, p 254–261
22. G. Hu, H.M. Meng, and J.Y. Liu, Microstructure and Corrosion Resistance of Induction Melted Fe-Based Alloy Coating, *Surf. Coat. Technol.*, 2014, **251**, p 300–306
23. Q.L. Yuan, X.D. Feng, and G.L. Ji, Comparative Analysis on the Microstructure and Property of Ni-Based Coatings Remelted by Laser and Flame, *J. Comput. Theor. Nanostruct.*, 2012, **9**, p 1347–1351
24. J. Iwaszko, K. Kudla, and M. Szafarska, Remelting Treatment of the Non-conductive Oxide Coatings by Means of the Modified GTAW Method, *Surf. Coat. Technol.*, 2013, **50**, p 322–327
25. X.H. Wang, Z.D. Zou, S. Song, and S.Y. Qu, Microstructure and Wear Properties of In Situ TiC/FeCrBSi Composite Coating Prepared by Gas Tungsten Arc Welding, *Wear*, 2006, **260**, p 705–710
26. X. Luo, J. Li, and G.J. Li, Effect of NiCrBSi Content on Microstructural Evolution, Cracking Susceptibility and Wear Behaviors of Laser Cladding WC/Ni-NiCrBSi Composite Coatings, *J. Alloys Compd.*, 2015, **626**, p 102–111
27. H.J. Liu, *Welding Metallurgy and Weldability Books*, Machinery Industry Press, Beijing, 2007
28. M. Eriksen, The Influence of Die Geometry on Tool Wear in Deep Drawing, *Wear*, 1997, **207**, p 10–15
29. C.B. Wang, *Tribological Materials and Surface Engineering Books*, National Defense Industry Press, Beijing, 2012